Influence of surface features on the adhesion of *Staphylococcus epidermidis* to Ag–TiCN thin films

Isabel Carvalho, Mariana Henriques, João Carlos Oliveira, Cristiana Filipa Almeida Alves, Ana Paula Piedade & Sandra Carvalho

Influence of surface features on the adhesion of *Staphylococcus epidermidis* to Ag–TiCN thin films

Isabel Carvalho[1,2]**, Mariana Henriques**[2]**, João Carlos Oliveira**[3]**, Cristiana Filipa Almeida Alves**[1]**, Ana Paula Piedade**[3] **and Sandra Carvalho**[1,3]

[1] GRF-CFUM, University of Minho, Campus of Azurém, 4800-058 Guimarães, Portugal
[2] IBB—Institute for Biotechnology and Bioengineering Centre for Biological Engineering, University of Minho, Campus of Gualtar, 4700-057, Portugal
[3] CEMUC Mechanical Engineering Department, University of Coimbra, 3030-788 Coimbra, Portugal

E-mail: isascarvalho@hotmail.com

Abstract

Staphylococcus epidermidis has emerged as one of the major nosocomial pathogens associated with infections of implanted medical devices. The initial adhesion of these organisms to the surface of biomaterials is assumed to be an important stage in their colonization. The main objective of this work is to assess the influence of surface features on the adhesion of *S. epidermidis* to Ag–TiCN coatings deposited by dc reactive magnetron sputtering. The structural results obtained by x-ray diffraction show that the coatings crystallize in a B1-NaCl crystal structure typical of $TiC_{0.3}N_{0.7}$. The increase of Ag content promoted the formation of Ag crystalline phases. According to the results obtained with atomic force microscopy, a decrease on the surface roughness of the films from 39 to 7 nm is observed as the Ag content increases from 0 to 15 at.%. Surface energy results show that the increase of Ag promotes an increase in hydrophobicity. Bacterial adhesion and biofilm formation on coatings were assessed by the enumeration of the number of viable cells. The results showed that the surface with lower roughness and higher hydrophobicity leads to greater bacterial adhesion and biofilm formation, highlighting that surface morphology and hydrophobicity rule the colonization of materials.

Keywords: sputtering, microorganism adhesion, biofilm, hydrophobicity, biomaterial

1. Introduction

Nowadays, the use of biomaterials is becoming increasingly common for the total or partial replacement of human organs and tissues. Nevertheless, these materials are susceptible to microbial colonization. Adhesion of bacteria to human tissue and implanted biomaterial surfaces is an important step in the infection process [1]. *Staphylococcus epidermidis*, a coagulase-negative staphylococcus, colonizes the skin and mucous membranes of the human body, representing an important part of its normal microflora [2, 3]. It has emerged in the last few years as the most frequently isolated pathogen in nosocomial sepsis associated with prosthetic device-related infection [4]. *S. epidermidis* has the ability to adhere to biomaterial surfaces and develop biofilms. Adhesion phenomena are a complex process, affected by numerous factors, such as surface properties of bacteria, material surface properties and environmental conditions [1, 5].

Table 1. Chemical composition, deposition parameters, thickness and deposition rate of deposited coatings.

Samples Ag/Ti	Chemical Composition (at.%)					[a] ΦN_2 (sccm)	[a] ΦC_2H_2 (sccm)	Current density (mA cm^{-2})		Thickness (μm)	Deposition rate (μm h^{-1})
	Ti	C	N	O	Ag			Ti	Ti + Ag		
0	39	22	34	5	0	5	2	10	0	2.8 ± 0.1	1.6
0.37	27	20	38	5	10	4	1.7	5.2	3.7	1.8 ± 0.2	1.1
0.62	24	22	36	3	15	3	1.2	3.5	3	2.5 ± 0.3	1.5

[a.] Gas flow.

In the adhesion process, bacteria firmly adhere to the biomaterial surface through physicochemical interactions [6]. Consequently, hydrophobicity, roughness and chemical composition of the biomaterial surface are important properties in the adhesion phenomenon [7]. Thus, it is fundamental to develop surfaces with optimized properties that are able to prevent microbial colonization. Besides presenting improved biological properties, these biomaterials also need to present enhanced physical, mechanical or tribological properties. In recent years, nanocomposite protective films based on the combination of various transition metal nitrides, carbides and carbonitrides have gained popularity due to their superior mechanical and tribological properties [8–11]. Among these materials, titanium carbonitride (TiCN) has been studied in the last few decades especially in what concerns the relation between structural properties and their mechanical and tribological behaviour. TiCN presents excellent wear resistance, high hardness and good corrosion resistance beyond its non-cytotoxic character [8, 12, 13].

Several researchers have used silver as an antibacterial element aiming at the reduction of microorganism colonization which is responsible for medical device failure [14–17]. The mechanism of the action of silver on microbes is still not clear, but it is suggested that silver ions act by strongly binding to critical biological molecules (proteins, DNA, RNA) and disrupting their functions [18–20].

So, the aim of this work is to assess the surface properties ruling adhesion of *S. epidermidis* to Ag–TiCN coatings produced by dc reactive magnetron sputtering for hip implant applications. With this research we intend to get more insight into the mechanism of microbial adhesion. The chemical, physical and biological analyses are correlated with the evolution of the ratio of Ag/Ti inside the coatings.

2. Materials and methods

2.1. Samples preparation and chemical composition

Ag–TiCN samples were prepared by dc reactive unbalanced magnetron sputtering using two targets, Ti and Ti/Ag, in an Ar, C_2H_2 and N_2 atmosphere. Silver pellets were placed in the preferential erosion area of one Ti target in order to obtain Ag contents up to 15 at.%. The base pressure in the chamber was 8×10^{-4} Pa and rose up to 2×10^{-1} Pa after Ar, N_2 and C_2H_2 gases were introduced. The coatings were deposited onto 316L stainless steel 20×20 mm for biological assays and single-crystal silicon (100) 10×10 mm substrates

for structural analysis. During depositions, the substrates were spaced 70 mm from the targets and were rotated at a constant speed of 7 rpm to ensure the deposition of homogeneous films. The temperature within the chamber as well as the bias voltage was kept constant at 373 K and −50 V, respectively. Argon flow was kept at 60 sccm, while the reactive gas fluxes, C_2H_2 and N_2, varied as indicated in table 1. The current density applied to the targets was adjusted in order to obtain different Ag/Ti atomic ratios, while the reactive gas fluxes were tuned to maintain similar C and N contents in all the films.

The chemical composition of the deposited films was measured using Cameca, Camebax SX 50, electron probe microanalysis equipment.

2.2. Physical characterization

Ball crater tests were performed with a 15 mm diameter sphere rotating at 700 rpm during 80 s. The film thickness was calculated from the diameters of the rings.

Hydrophobicity parameters of surfaces were determined through the sessile drop contact angle technique, using an automated contact angle measurement apparatus (OCA 15 Plus; Dataphysics, Germany). Cleaned and dried surfaces were used for determining the hydrophobicity parameters of Ag–TiCN coatings. All measurements were performed at room temperature, and water, formamide and α-bromonaphtalene, with known surface energy components [21, 22], were used as reference liquids. Contact angle measurements allowed the calculation of substrata hydrophobicity parameters using the van Oss approach [23].

2.3. Structural characterization

The structure and phase distribution of the coatings were determined by x-ray diffraction (XRD) using a Siemens diffractometer in a Bragg–Brentano geometry and Co Kα radiation (1.788 97 Å).

The grain sizes were calculated applying the Scherrer equation after a nonlinear Voigt curve fit on the (111) peaks of the diffractograms using OriginPro 8 software.

The chemical bonds were evaluated by micro-Raman spectroscopy. Raman spectra were acquired with a Renishaw InVia microscope using the 514.5 nm Ar laser line.

2.4. Morphology and topography

The morphology of the coatings was assessed by scanning electron microscopy (EDAX-Nova nanoSEM 200) in both
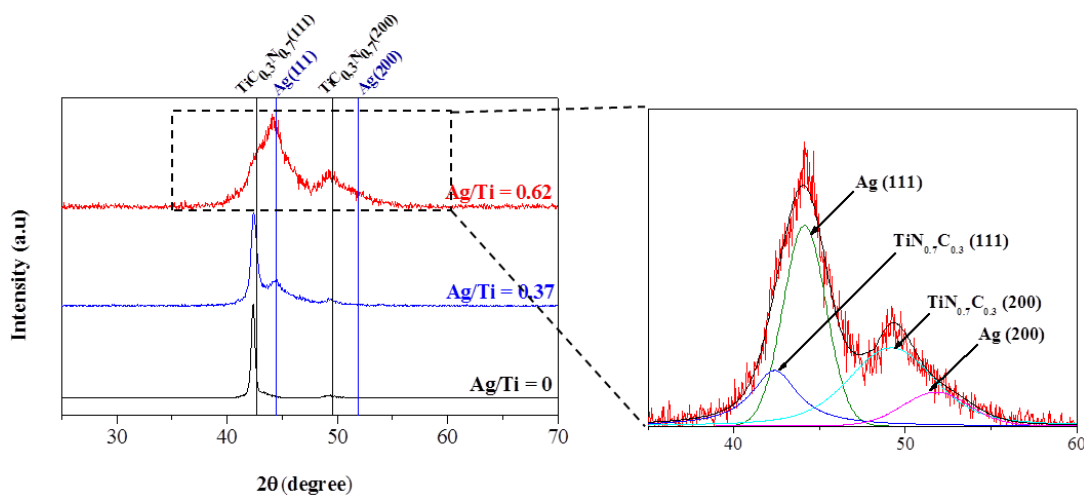
Figure 1. XRD patterns of the Ag–TiCN coatings deposited by dc reactive magnetron sputtering and in the right the deconvolution of peak Ag/Ti = 0.62.

backscattering (BSE) and secondary electron (SE) modes, while surface roughness and topography were characterized by atomic force microscopy (AFM NanoScope III Digital Instruments). The roughness measurements were performed under a scan range of $5 \times 5 \, \mu$m in tapping mode. Measurements were made in three areas randomly chosen in all samples.

2.5. Biological assays

Bacterial colonization assays were performed using two strains of *S. epidermidis*, IE186 and 1457. The strains were stored at $-80\,^{\circ}$C in glycerol stocks. Cells were firstly grown for approximately 36 h in plates of Tryptic Soy Agar (TSA, Merck), and then incubated for 18 h in Tryptic Soy Broth (TSB, Merck), at $37\,^{\circ}$C under a constant agitation of 120 rpm. After this period, cells were centrifuged for 5 min at 8900g and $4\,^{\circ}$C and washed twice with a phosphate buffer saline (PBS 1$\times$). The cellular suspension was adjusted to a final concentration of approximately 1×10^8 cells ml^{-1}, determined by optical density at 640 nm, prior to usage in the adhesion and biofilm formation assays. Coated coupons (previously sterilized at $121\,^{\circ}$C for 15 min) were inserted in six-well plates and 3 ml of cellular suspension was added to each well. The plates with the materials were then incubated at $37\,^{\circ}$C under a constant agitation of 120 rpm for 2 and 24 h.

After incubation of *S. epidermidis* strains, the coatings were gently washed with PBS to remove non-attached bacteria. Thereafter the adherent bacteria were detached from the coatings using an ultrasonic bath for 10 min. The bacteria were incubated with serial dilutions on TSB agar plates at $37\,^{\circ}$C for 24 h, and then the number of CFUs was counted. All experiments were done in triplicate and repeated at least in two independent assays.

Scanning electron microscopy was used to observe bacteria adhesion and biofilm formation on the surface of the coatings. After adhesion and biofilm formation the coatings were carefully washed three times with distilled water. Samples were dehydrated by an immersion in increasing

ethanol concentration solutions: 70, 95 and 100% (v/v) for 10, 10 and 20 min, respectively, and placed in a sealed desiccator. Afterwards, the samples were mounted on aluminium bases with carbon tape, sputter-coated with gold and observed with a Leica S360 scanning electron microscope. In order to assess the extent of bacterial adhesion and biofilm formation in each sample, three fields were used for image analysis. All photographs were taken using a magnification of 1000$\times$.

2.6. Statistical analysis

Results from biological assays were compared using one-way analysis of variance by applying the Bonferroni multiple comparisons test, using the software Statistical Package for the Social Sciences Inc. (SPSS). All tests were performed with a confidence level of 95%.

3. Results and discussion

3.1. Chemical composition

The chemical composition, thickness and some experimental details of the coatings are summarized in table 1. Increasing the J_{Ti+Ag}/J_{Ti} current density ratio promoted an increase in Ag content from 0 to 15 at.%, while the Ti content decreased from 39 to 24 at.%. Similar carbon and nitrogen contents were measured in all the films and oxygen contamination was in the range of 3–5 at.%.

3.2. Structural analysis

Figure 1 shows the XRD diffraction patterns for the deposited coatings with three different Ag/Ti atomic ratios (0, 0.37 and 0.62) and the lattice parameters (*a*). The reference peaks, obtained from the International Centre for Diffraction Data (ICDD) database, for TiC$_{0.3}$N$_{0.7}$ (ICDD card no. 00-042-1488) and Ag (ICDD card no. 00-004-0783), are also included at the top of figure 1. The differences in the composition are well correlated with those observed in the

structure evolution. In fact, the film without silver crystallizes in a B1-NaCl crystal structure typical for $TiC_{0.3}N_{0.7}$. The diffraction peaks at $2\theta = 42.39°$ and $49.32°$ were assigned to the (111) and (200) planes of $TiC_{0.3}N_{0.7}$, respectively. Both peaks are shifted to lower angles as compared to the reference values, as a result of a lattice parameter slightly higher than the standard value ($a = 4.26$ Å). This result may be related to higher C/N atomic ratio in the film than in standard $TiC_{0.3}N_{0.7}$, as observed in a previous study [24]. Moreover, the shift of the XRD peaks towards lower angles may be due to the development of compressive residual stresses which are often associated with the deposition process [13].

The B1-NaCl crystal structure typical of $TiC_{0.3}N_{0.7}$ is also detected in the film deposited with a 0.37 Ag/Ti atomic ratio, along with a new diffraction peak close to $2\theta = 44.35°$ which was assigned to fcc-Ag (111). The $TiC_{0.3}N_{0.7}$ diffraction peaks become broader with silver incorporation in the films, concurrently with the development of the characteristic pattern of metallic silver. The XRD pattern of the sample deposited with a 0.62 Ag/Ti atomic ratio displays two broad diffraction peaks. Deconvolution of the higher intensity band resulted in two peaks, at $42.44°$ and $44.19°$, which were attributed to $TiC_{0.3}N_{0.7}$ (111) and Ag (111), respectively. Deconvolution of the diffraction band at higher 2θ angles (between $48°$ and $53°$) also resulted in two peaks that were indexed to $TiC_{0.3}N_{0.7}$ (200) and Ag (200).

The grain size of TiC_yN_{1-y} and Ag phases was determined by Scherrer's formula using the (111) peak. The calculated values varied from 32 down to 5 nm and from 19 up to 29 nm with the increase of Ag content, for TiC_yN_{1-y} and Ag phases, respectively. This variation is concomitant with the increase of Ag content in the films, which results in the predominance of the fcc-Ag phase, while the degree of structural order of the TiCN phase decreases. The loss of crystallinity of the TiCN phase can be explained by two different mechanisms: (i) the growth interruption of the TiCN phase can be affected by the nucleation of Ag nanocrystals or (ii) by the increase of (C + N)/Ti atomic ratio as a consequence of the silver incorporation which leads to the formation of an amorphous layer, a-(C, CN_x) as reported by several authors for TiCN films also deposited by sputtering [10, 24–26].

Figure 2 shows the Raman spectra of deposited Ag–TiCN samples with different Ag/Ti ratio. For the samples with 0 and 0.37 Ag/Ti atomic ratio two weak and broad bands are detected in the ranges of 200–350 and 500–700 cm^{-1}. These bands correspond to acoustic and optical vibrational modes of titanium nitride/carbide, respectively [27–30]. According to another study [24], the TiCN bonds should be located between TiN and TiC bands. These results agree well with the XRD patterns as crystalline TiCN was detected for both samples. For the samples deposited with 0.37 and 0.62 Ag/Ti atomic ratio, two broad intense bands were detected between 1200 and 1700 cm^{-1}. These bands are assigned by several authors [31–33] to carbon-based phases such as D and G bands of carbon materials at 1332 and 1580 cm^{-1}, respectively [32]. Also, C–N vibrational modes have been reported in this region [31]. These results agree well with the formation of an amorphous phase, a-(C, CN_x), already
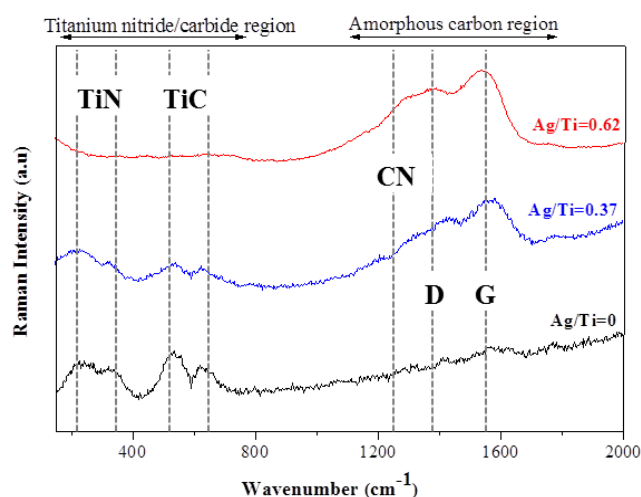

Figure 2. Raman spectra of the Ag–TiCN coatings.

suggested by the analysis of the XRD patterns. The (C + N)/Ti atomic ratio is the highest in the sample deposited with the highest Ag content which also shows more intense Raman peaks in the 1200–1700 cm^{-1} range. The higher amount of amorphous phase in this coating is responsible for the significant loss of crystallinity of the TiCN phase detected by XRD.

3.3. Morphology and topography analysis

The morphology and topography of the coatings were studied by cross-sectional SEM micrographs of fractured samples (figure 3). The cross-section of the sample without silver (figure 3(a)) shows an open columnar-type structure which terminates in domes at the surface. This structure presents high porosity, as shown in the inset of figure 3(a), in agreement with zone 1 of the Thornton model [34]. The low deposition temperature (373 K) as compared to the melting temperature of the deposited material which must be between the melting temperature of TiN and TiC (3203 K and 3413 K, respectively [35, 36]), and the low bombardment conditions used in this work resulted in reduced adatom mobility and subsequent formation of a porous structure [24]. The incorporation of Ag (Ag/Ti atomic ratio of 0.37) resulted in a denser film (figure 3(b)) although the columnar structure is retained. The inset in this figure, obtained in BSE mode, clearly shows the formation of Ag nanoclusters dispersed all over the film surface. Increasing the Ag content (Ag/Ti atomic ratio of 0.62) resulted in a further densification of the film and an increase in the number of Ag nanoclusters (figure 3(c)). Although the Ag nanoclusters are dispersed all over the film surface, inset in BSE mode, those formed in the porous zones of the film attained bigger sizes. The columnar growth observed in other thin films is no longer detected, which agrees well with the loss of crystallinity of the TiCN phase and simultaneous formation of an amorphous phase as suggested by XRD and Raman results.

The surface topography of samples was analysed by AFM (figure 4). The coating deposited without
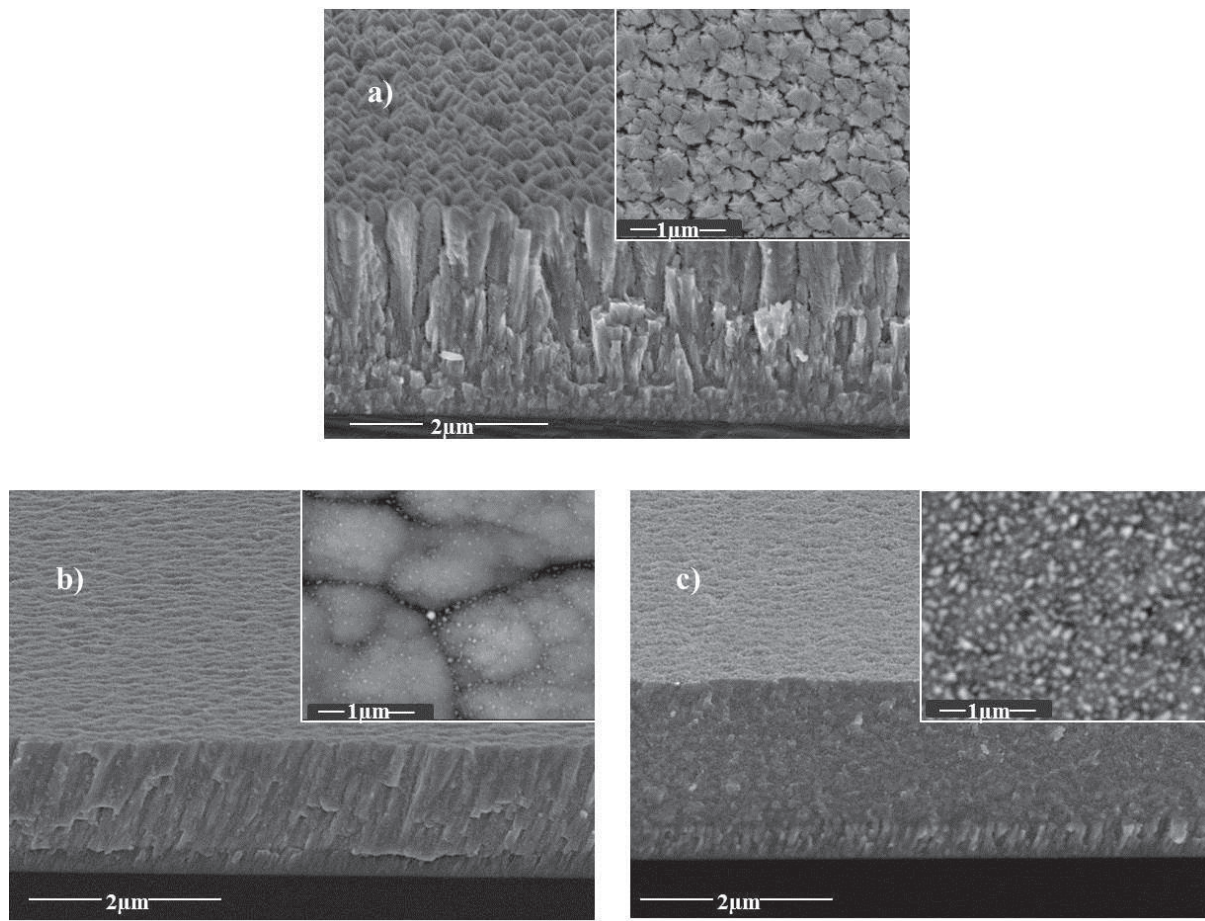
Figure 3. Cross-sectional SEM micrographs of coatings: (a) Ag/Ti = 0, (b) Ag/Ti = 0.37 and (c) Ag/Ti = 0.62. The insets show the SEM image from the sample surface where in (a) the top of column TiCN is evident and in (b) and (c) Ag clusters are visible (BSE image).
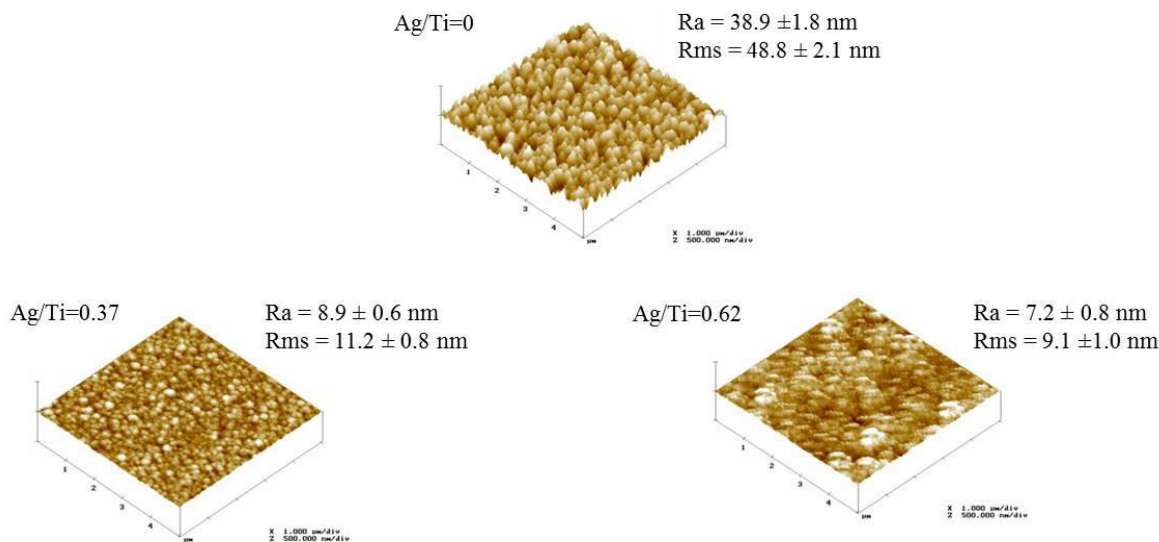
Figure 4. AFM images of coatings with a scan range of $5 \times 5 \, \mu$m. R_a is the arithmetic mean of surface roughness of every measurement within the total distance $1/2$ roughness average and rms is the root mean square roughness.

Ag has a roughness considerably higher than coatings deposited with Ag, as shown in figure 4. These results are in agreement with the film densification observed by SEM.

3.4. Surface hydrophobicity analysis

The hydrophobicity of the Ag–TiCN coating surfaces was evaluated through contact angle measurements, using the

Table 2. Water (θ_W), formamide (θ_F) and α-bromonaphtalene ($\theta_{\alpha-B}$) contact angles, surface energy components (apolar Lifshitz–van der Waals surface free energy component, γ^{LW}; electron acceptor surface free energy component, γ^+; and electron donor surface free energy component, γ^-), and degree of hydrophobicity (ΔG_{mwm}) of the Ag–TiCN coatings surface.

| Sample Ag/Ti	Contactangle $\pm$ SD[a] (deg)			Surface energy components (mJ m^{-2})			ΔG_{mwm} mJ m^{-2})
	θ_W	θ_F	$\theta_{\alpha-B}$	γ^{LW}	γ^+	γ^-	
0	112.6 ± 2.9	60.7 ± 2.6	74.1 ± 2.7	18.0	9.0	0.0	-41.7
0.37	99.3 ± 2.4	78.5 ± 2.0	65.1 ± 1.4	22.4	0.2	1.3	-70.6
0.62	114.6 ± 2.0	102.0 ± 1.7	91.5 ± 4.5	10.5	0.0	1.1	-82.3

[a] Standard deviation.
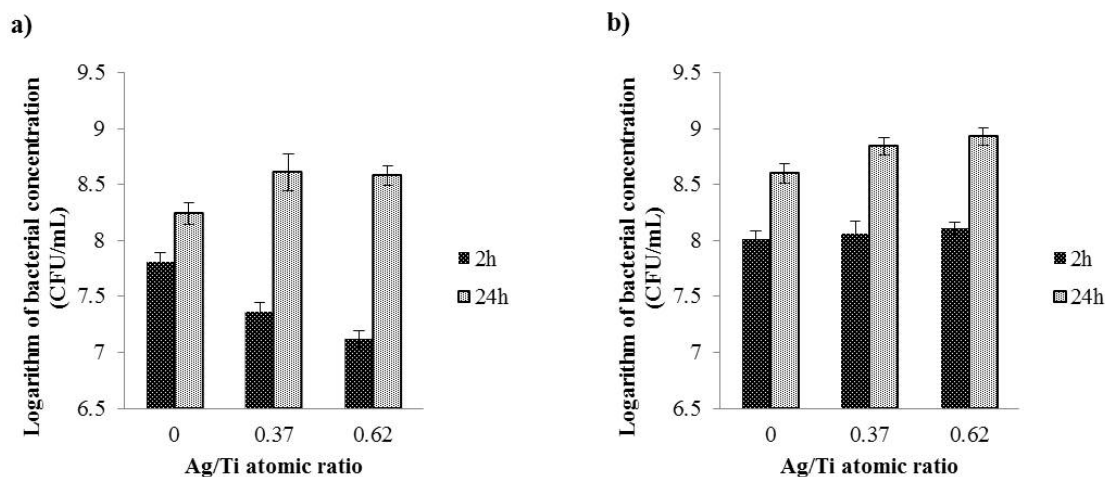
Figure 5. Logarithm of bacterial concentration after 2 and 24 h contact between Ag–TiCN coatings and the *S. epidermidis* strain: (a) IE186 and (b) 1457.

van Oss approach [23]. According to the approach, the hydrophobicity of a given material is defined in terms of the variation of the free energy of interaction (ΔG) between the material's surface (m) immersed in water (w), ΔG_{mwm}. When ΔG_{mwm} is negative, the free energy of interaction between molecules is attractive, revealing a greater interaction with each other than with water, making the material surface hydrophobic. In contrast, a surface is hydrophilic when ΔG_{mwm} is positive. Contact angles, surface energy parameters and the degree of hydrophobicity of coatings are presented in table 2.

The water contact angles obtained for the coating surfaces are higher than 90°, suggesting a hydrophobic character [37, 38], also confirmed by the negative values of ΔG_{mwm}. These coatings present a monopolar surface ($\gamma^+ = 9$ mJ m^{-2} and $\gamma^- = 0$ mJ m^{-2}) and the coatings with Ag present a slightly polar surface, both surface energy component values (γ^+ and γ^-) are quite close to zero, and this fact may highlight the surfaces' high densities of apolar areas which may promote the adhesion of microorganisms to those coatings with Ag [39]. The hydrophobic character of these coatings may result from the incorporation of silver preferentially in the grain boundaries, which lessens the roughness of coatings and makes them more homogeneous topographically.

3.5. Biological analysis

To assess the number of viable cells, the cellular concentration was determined by CFU (figure 5) in terms of the logarithm of bacterial concentration (CFU ml^{-1}) for each *S. epidermidis* strain (IE186, figure 5(a) and 1457, figure 5(b)). The selection of these two strains was based on their propensity to form biofilms in previous studies [40, 41]. According to the study of Sousa *et al* [40] 1457 strain produces a larger amount of extracellular polymeric substances (EPS) than IE 186. These substances are components of the biofilm matrix and consist mainly of polysaccharides and proteins [42]. The extracellular matrix is very important for intercellular binding during surface colonization [43] and protection against the host immune system and resistance to antibiotics [1]. Figure 5(a) shows that the addition of silver to TiCN coatings promotes a statistically significant decrease ($P < 0.05$) in bacterial adhesion. Nevertheless, this decrease does not represent antibacterial activity since the difference in the logarithmic value of viable cell counts between TiCN coatings with and without silver incorporation is not higher than 2.0. According to the Japanese Industrial Standard Z 2801: 2000 [44], if the difference in the logarithmic value of viable cells counts between antimicrobial products and untreated products is less than 2.0, antimicrobial activity cannot be considered. Regarding the strain 1457, it is possible to observe (figure 5(b)) that with increasing silver concentration
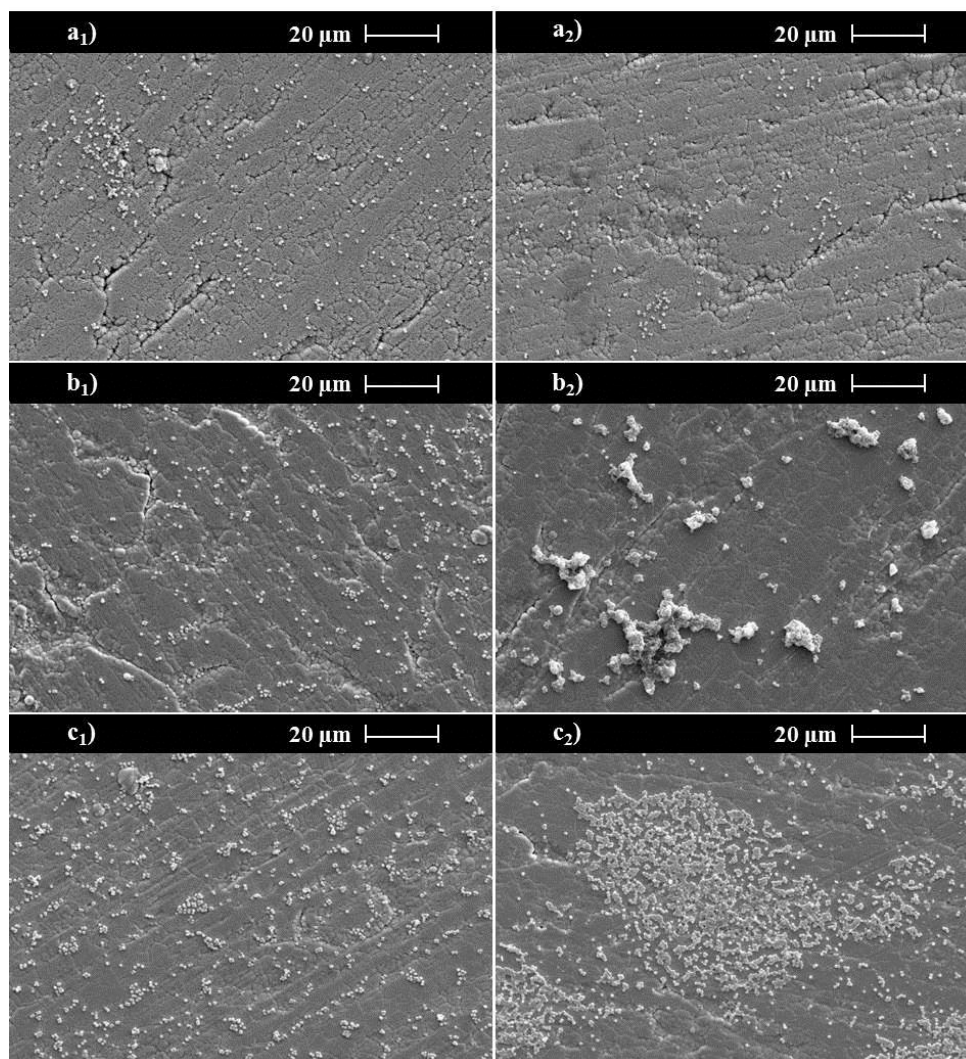
Figure 6. SEM micrographs of *S. epidermidis* IE186 adhered to Ag–TiCN coatings after 2 and 24 h periods of contact: adhesion and biofilm formation to Ag/Ti = 0 (a_1) and (a_2), respectively; to Ag/Ti = 0.37 (b_1) and (b_2), respectively; to Ag/Ti = 0.62 (c_1) and (c_2), respectively.

the increase in bacteria adhesion (2 h) is not statistically significant ($P > 0.05$). The results of the biofilm formation (24 h) for both strains show that the addition of silver in the coatings promotes a statistically significant increase ($P < 0.05$) in bacterial concentration. This fact was not expected since silver is known for its antibacterial effect [18–20, 45, 46]. Based on studies of Sousa *et al* [5] and Cerca *et al* [41], *S. epidermidis* IE186 and 1457 are hydrophilic, with $\Delta G_{mwm} > 0$, and both strains show a preference to attach to hydrophobic surfaces. As previously reported, the hydrophobic behaviour of the coatings seems to promote a favourable bacterial adhesion. Ag–TiCN coatings with Ag/Ti atomic ratios of 0.37 and 0.62 possess sites with high densities of apolar areas that can justify the bacterial adhesion to the surface via the hydrophobic effect.

SEM images presented in figures 6 and 7 confirm that silver seems to have no antibacterial action and it is possible to confirm that biofilm formed by 1457 is greater than IE186 strains. These results may be due to the amount of ionic silver released from the surfaces, which may be insufficient or even

non-existent. In fact, SEM images reveal that silver coatings seem to favour adhesion and biofilm formation. This can be explained by the morphology of the coatings and/or by their hydrophobicity characteristics.

The introduction of silver causes the formation of a second crystalline phase (fcc-Ag), which usually tends to develop in the grain boundaries, increasing the contact opportunities between bacteria and surface coatings (figure 8); as the non-silver coatings have a columnar structure with a width of approximately 300 nm ($L = 283.20$ nm) (figure 9) and as these bacteria have a diameter of around 1 μm, the contact opportunities between bacteria and these surfaces are lower than for the surfaces with silver.

Indeed, as silver produces no antibacterial effect, one is lead to believe that this element is in its metallic form and its ionization does not happen or occurs at very low concentrations which do not cause the death of the bacteria. In a previous study [24], the analysis of Ag 3d photoelectron spectra applied in similar samples to the ones used in this work, showed that the only contribution was of Ag–Ag metal bonds.
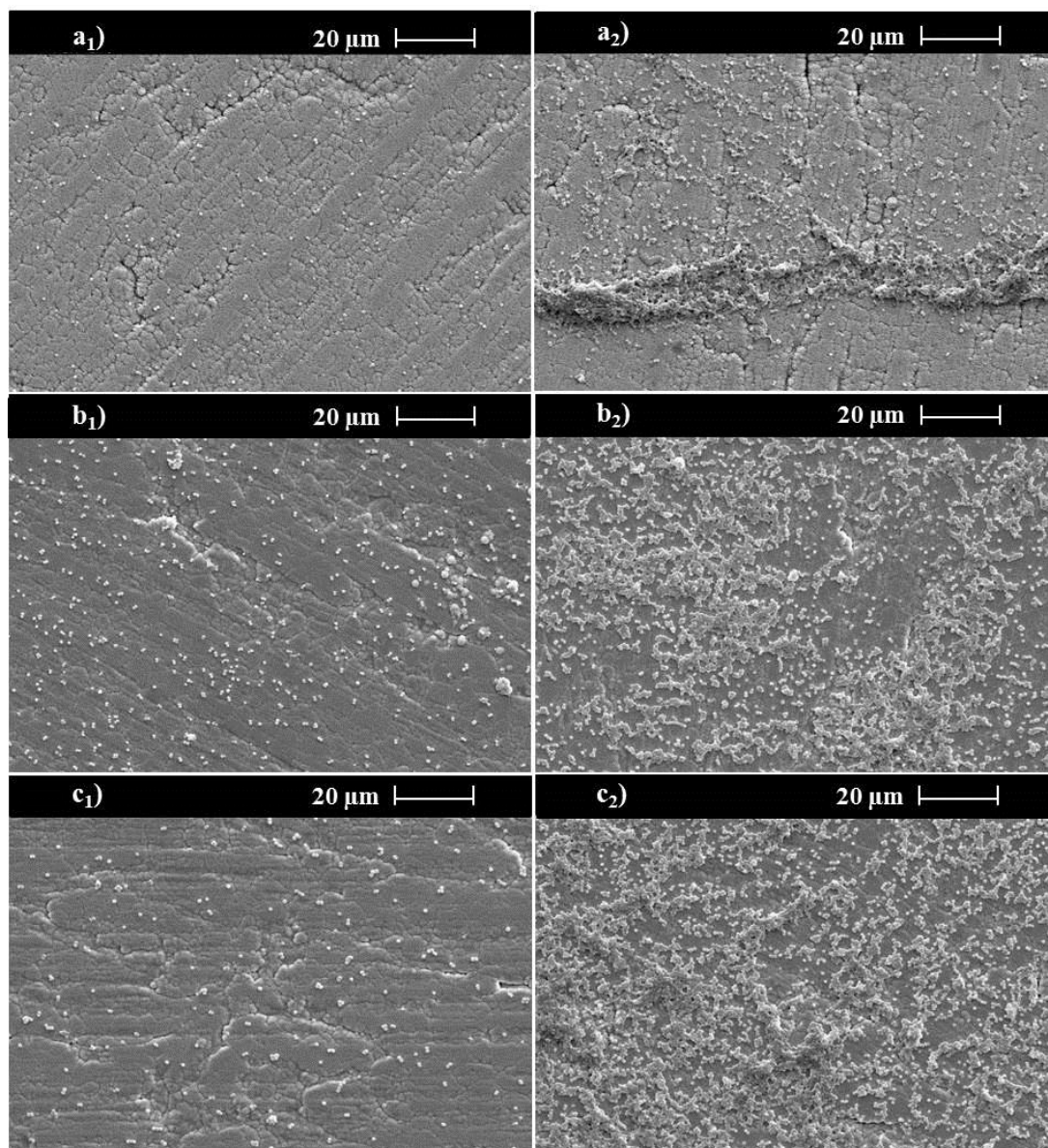
Figure 7. SEM micrographs of *S. epidermidis* 1457 adhered to Ag–TiCN coatings after 2 and 24 h periods of contact: adhesion and biofilm formation to Ag/Ti = 0(a_1) and (a_2), respectively; to Ag/Ti = 0.37(b_1) and (b_2), respectively; to Ag/Ti = 0.62(c_1) and (c_2), respectively.
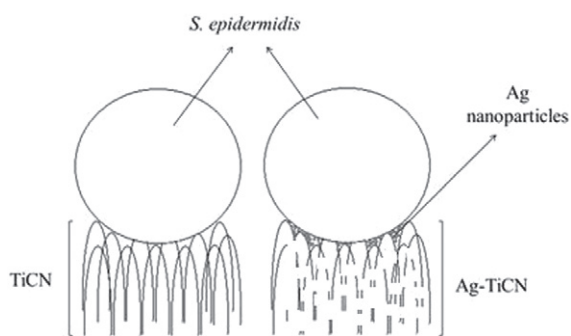
Figure 8. Schematic of bacterial adhesion (not to scale).

4. Conclusions

Ag–TiCN thin films were deposited by reactive magnetron sputtering with different Ag/Ti atomic ratios (0, 0.37 and 0.62) which affect the structure evolution. Samples with Ag/Ti atomic ratios of 0 and 0.37 crystallize in a B1-NaCl crystal structure typical of $TiC_{0.3}N_{0.7}$. A second crystalline phase begins to appear with Ag/Ti atomic ratios of 0.37, becoming dominant with Ag/Ti atomic ratios of 0.62. Simultaneously, amorphous carbon-based phases also develop, as confirmed by Raman spectroscopy. Silver phases and a-(C, CN_x) tend to segregate in the grain boundaries of $TiC_{0.3}N_{0.7}$ causing a reduction in the grain size and a
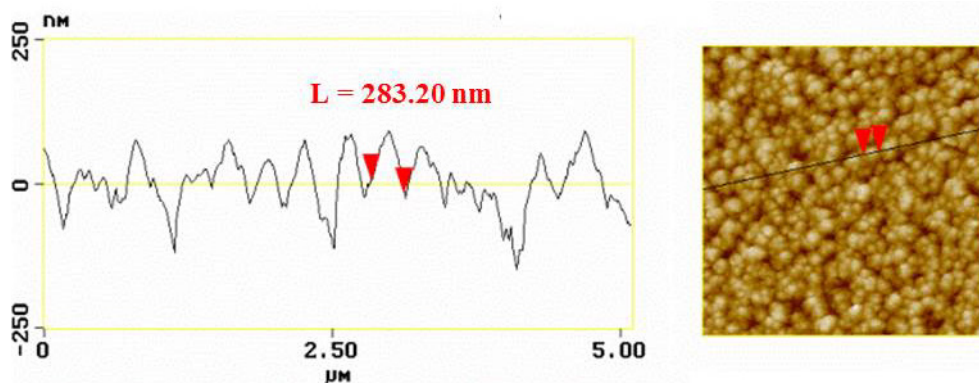
Figure 9. AFM section profile obtained on Ag–TiCN coating with zero Ag/Ti atomic ratio.

densification of the coatings, resulting in a higher number of contact zones between the bacteria and the film surface. Increasing silver in coatings leads to less rough and more hydrophobic surfaces. The hydrophobic behaviour of the coatings promotes favourable bacterial adhesion. Ag–TiCN coatings with Ag/Ti atomic ratios of 0.37 and 0.62 possess sites with high densities of apolar areas that can justify the bacterial adhesion to the surface via the hydrophobic effect.

Acknowledgments

References

[1] An Y H and Friedman R J 1998 *J. Biomed. Mater. Res.* **43** 338–48

[2] Vuong C and Otto M 2002 *Microbes Infection/Institut Pasteur* **4** 481–9

[3] O'Gara J P and Humphreys H 2001 *J. Med. Microbiol.* **50** 582–7

[4] Fitzpatrick F, Humphreys H, Smyth E, Kennedy C A and O'Gara J P 2002 *J. Hosp. Infection* **42** 212–8

[5] Sousa C, Teixeira P and Oliveira R 2009 *Int. J. Biomater.* **2009** 718017

[6] Oliveira R, Azeredo J and Teixeira P 2003 *The Importance of Physicochemical Properties in Biofilm Formation and Activity* ed S Wuertz, P Bishop and P Wilderer (London: IWA) pp 211–31

[7] Tang H, Cao T, Liang X, Wang A, Salley S O, McAllister J and Ng K Y S 2009 *J. Biomed. Mater. Res.* A **88** 454–63

[8] Serro A P, Completo C, Colaço R, Dos Santos F, Da Silva C L, Cabral J M S, Araújo H, Pires E and Saramago B 2009 *Surf. Coat. Technol.* **203** 3701–7

[9] Oliveira C *et al* 2008 *Surf. Coat. Technol.* **203** 490–4

[10] Silva E, Rebelo de Figueiredo M, Franz R, Galindo R E, Palacio C, Espinosa A, Calderon S V, Mitterer C and Carvalho S 2010 *Surf. Coat. Technol.* **205** 2134–41

[11] Carvalho S, Rebouta L, Ribeiro E, Vaz F, Tavares C J, Alves E, Barradas N P and Riviere J P 2009 *Vacuum* **83** 1206–12

[12] Bahl R, Kumar A, Vedawyas M and Patel D 1999 *Appl. Phys.* A **69** 643–6

[13] Sánchez-López J C, Abad M D, Carvalho I, Escobar Galindo R, Benito N, Ribeiro S, Henriques M, Cavaleiro A and Carvalho S 2012 *Surf. Coat. Technol.* **206** 2192–8

[14] Endrino J L, Anders A, Albella J M, Horton J A, Horton T H, Ayyalasomayajula P R and Allen M 2010 *J. Phys.: Conf. Ser.* **252** 012012

[15] Böswald M, Mende K and Bernschneider W 1999 *Infection* **27** 38–42

[16] Kelly P J, Li H, Whitehead K A, Verran J, Arnell R D and Iordanova I 2009 *Surf. Coat. Technol.* **204** 1137–40

[17] Chiang W-C, Tseng I-S, Møller P, Hilbert L R, Tolker-Nielsen T and Wu J-K 2010 *Mater. Chem. Phys.* **119** 123–30

[18] Morones J R, Elechiguerra J L, Camacho A, Holt K, Kouri J B, Ramírez J T and Yacaman M J 2005 *Nanotechnology* **16** 2346–53

[19] Rai M, Yadav A and Gade A 2009 *Biotechnol. Adv.* **27** 76–83

[20] Feng Q, Wu J and Chen G 2000 *J. Biomed. Mater. Res.* **52** 662–8

[21] Janczuk B, Chibowski E, Bruque J, Kerkeb M and Caballero F 1993 *J. Colloid Interface Sci.* **159** 421–8

[22] Oliveira R, Azeredo J, Teixeira P and Fonseca A P 2001 *The Role of Hydrophobicity in Bacterial Adhesion* ed P Gilbert, D Allison, M Brading, J Verran and J Walker (Cardiff: BioLine) pp 11–22

[23] van Oss C J and Giese R F 1995 *Clays Clay Miner.* **43** 474–7

[24] Manninen N K, Galindo R E, Benito N, Figueiredo N M, Cavaleiro A, Palacio C and Carvalho S 2011 *J. Phys. D: Appl. Phys.* **44** 375501

[25] Lu Y H and Shen Y G 2011 *J. Mater. Res.* **22** 2460–9

[26] Martínez-Martínez D, Sánchez-López J C, Rojas T C, Fernández A, Eaton P and Belin M 2005 *Thin Solid Films* **472** 64–70

[27] Oliveira C, Galindo R E, Palacio C, Vázquez L, Espinosa A, Almeida B G, Henriques M, Calderon S V and Carvalho S 2010 *Thin Solid Films* **518** 5694–9

[28] Constable C, Yarwood J and Münz W 1999 *Surf. Coat. Technol.* **119** 155–9

[29] Dreiling I, Haug A, Holzschuh H and Chassé T 2009 *Surf. Coat. Technol.* **204** 1008–12

[30] Spengler W, Kaiser R, Christensen A and Müller-Vogt G 1978 *Phys. Rev.* B **17** 1095–1101

9

[31] Ferrari A C, Rodil S E and Robertson J 2003 *Diamond Relat. Mater.* **12** 905–10

[32] Robertson J 2002 *Mater. Sci. Eng.* R **37** 129–281

[33] Escobar-Alarcon L, Medina V, Camps E, Romero S, Fernandez M and Solis-Casados D 2011 *Appl. Surf. Sci.* **257** 9033–7

[34] Thornton J A 1977 *Annu. Rev. Mater. Sci.* **7** 239–60

[35] Zhang S 1993 *Mater. Sci. Eng.* A **163** 141–8

[36] Simon J G and Langer E L 1994 *ASM Handbook Volume 5: Surface Engineering* (ASM International)

[37] Kapoor R and Eagar T 1989 *Metall. Mater. Trans.* B **20** 919–24

[38] Nascimento R M Do, Martinelli A E and Buschinelli A J A 2003 *Cerâmica* **49** 178–98

[39] Doyle R J 2000 *Microbes Infection/Institut Pasteur* **2** 391–400

[40] Sousa C, Teixeira P and Oliveira R 2009 *J. Basic Microbiol.* **49** 363–70

[41] Cerca N, Pier G B, Vilanova M, Oliveira R and Azeredo J 2005 *Res. Microbiol.* **156** 506–14

[42] Sutherland I W 2001 *Trends Microbiol.* **9** 222–7

[43] Donlan R M 2001 *Emerging Infectious Diseases* **7** 277–81

[44] Japanese Industrial Standard Z 2801 2000 *Antimicrobial Products—Test for Antimicrobial Activity and Efficacy* (Tokyo: Japanese Standards Association)

[45] Hsieh J, Tseng C, Chang Y, Chang S and Wu W 2008 *Surf. Coat. Technol.* **202** 5586–9

[46] Kelly P J, Li H, Benson P S, Whitehead K A, Verran J, Arnell R D and Iordanova I 2010 *Surf. Coat. Technol.* **205** 1606–10